Research Article

Energy, Environment and Storage (2024) 04-01:5-12

Energy, Environment and Storage

Journal Homepage: www.enenstrg.com

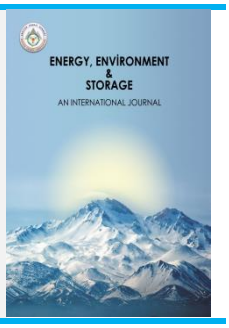

Vertical Axis Turbine Performance at Different Parameters: Effects of Generated Turbulence

Suleyman Osmanli[1,2*], S. Orhan Akansu[1], Y. Erkan Akansu[3]

[1]Erciyes University, Faculty of Engineering, Dept. of Mech. Eng. 38280, Kayseri, Turkey ORCID: 0000-0002-0085-7915
[2,]Van Yuzuncu Yil University, Faculty of Engineering, Dept of Mech. Eng., 65080, Van, Turkey ORCID: 0000-0001-8854-0332*
[3]Nigde Omer Halisdemir University, Faculty of Engineering, Dept of Mech. Eng., 51240, Nigde, Turkey ORCID: 0000-0003-0691-3225

ABSTRACT. The need to increase the energy efficiency and energy harvesting of vertical axis wind turbines is growing as a consequence of the quick expansion in the energy sector. Therefore, it is crucial to comprehend how a turbine operates. In this study, the more often used VAWT—vertical axis wind turbine—has been experimentally evaluated. Various performance graphs have been produced as a result. At various wind speeds, S1014 and S1020 airfoils are employed. Aspect ratio and angle of attack were noted, and the performance of the turbine was investigated in relation to the impact of the current produced by the turbulence generating plate. The subsonic wind tunnel setup utilized during the testing consisted of a 15 W DC motor and a 0.1 Nm torque meter. The findings demonstrated that the S1014 type blade profile was more efficient and boosted performance of the two types.

Keywords: VAWT, Turbulence, Efficiency, Sustainability, Energy.

Article History: Received: 22.07.2023; Accepted: 23.01.2024

Doi: https://doi.org/10.52924/VURM7594

1. INTRODUCTION

One of the most important issues of the current era, perhaps the most important is solving energy problems. It is gradually shifting towards sustainable energy due to energy diversity, reduction of fossil fuels, extraction costs and emission values to the environment. Therefore, there is a need for technologies that can obtain energy from nature that do not pollute the environment. Among these resources, wind power is developing rapidly and its usage area is increasing. Even in the future, the decrease in the production cost of the turbines per unit rather than the efficiency will be decisive for the use of this energy source.

The applications of small-scale wind turbines for electricity generation in rural areas are increasing. Naturally, both academic studies and commercial productions in this field are still increasing rapidly [1]. In general, wind types are divided into two as horizontal and vertical.

Although horizontal axis turbines are based on the principle of lift, they require relatively higher wind speeds. Vertical Axis Wind turbines, VAWTs are used for low-speed and low-noise areas for non-urban living spaces [2,3]. On the other hand, these systems can be installed to building in city center or special structures [4]. In some cases, researchers can place turbines in different locations. Krishnan and Paraschivoiu [11] used to obtain performance characteristics of rooftop vawt. They showed that the design of diffuse-shaped shroud provides high coefficient of performance. This type of turbines not only require lift but also works with drag force. VAWTs can be analyzed in three parts as Savonius, Darrieus and Helical [5,6]. It has been observed to be very effective in self-starting the Savonius-type turbine [7] and produces their torque at low angles of attack [8]. Darrieus was found as VAWT in the 1920s by F. M. Darrieus based on the principle of airplane aerodynamics. This principle includes different profile shape between upper and lower surface of the blade which caused lifting force by pressure difference [9]. VAWTs are unfortunately quite unsuccessful in self-starting. In order to overcome this, some studies that are used in combination with darrieus turbines are available [10]. In addition, because of the disadvantages of Darrieus VAWT over high performance and traditional horizontal axis wind turbines, the VAWT workspace is limited to unstable wind environments and analysis systems are complex [1].

Many studies have focused on increasing the VAWT's performance. [17-22]. These upgrades may primarily be divided into three groups: optimizing [23–25], adding a device [26–28], and utilizing aerodynamic interaction [29–33]. Experimental investigations have looked at performance factors in other research [12–16]. Their experimentation with several blade types suggests creating a hybrid turbine.

*Corresponding author: steksin@erciyes.edu.tr

The conflicting results of the recently published and previous research indicate that the VAWT rotor blade aerodynamics and kinematics are still not fully understood under changing wind conditions.

In this study, our aim observes the effect of turbulence on Vertical Axis Wind Turbine, VAWT and performance characteristics with two different blade profile. Many parameters were altered such as Angle of Attack, AoA, Aspect ratio, H/D, free stream velocity, $U_∞$. Comparisons were made with bare case and turbulent flow regime. Graphics are generated in TSR versus coefficient performance, Cp. Also, solidity effect was investigated. The experimental strategy is defined in Section 2, the results shown in Sections 3. In the last part, a short and concise summary of the whole study is given.

2. MATERIALS AND METHODS

This portion of the article goes into depth about the tools used in the wind tunnel and all the methods utilized to test and record VAWT performance. In this study, power output and other characteristics were examined with turbine blades. All experiments were done both in the Erciyes University, faculty of aeronautics and astronautics, subsonic wind tunnel and Nigde Omer Halisdemir University, Mechanical Engineering department aerodynamic flow control laboratory. Wind tunnel cross section has 570 x 570 mm dimensions at the entrance to test region and expands with 30 to kept constant the static pressure along the 1800 mm. 15 kW fan can reach 33 mm/s wind speed at the empty status. This subsonic wind turbine setup can be seen in figure 1.

Two different blade profiles *(S1014, S1020)* were used during the experiment. The span length, diameter of turbine, angle of attack, flow regime was altered in order to obtain power output by changing the electronically load. Rigol DL3021 brand device was used for this loading as shown in figure 2. Burster torqumeter was connected between turbine shaft and 15W Maxon DC motor.

Fig. 1. General view of the test facility.

8 channel Oros datalogger was used to collect data 1000 sampling frequency. Free stream wind velocity, $U_∞$, was measured at each case to minimize error due to the existence of turbine in the test section. Because, any obstacle in the test section can be caused 20% reduction on the free stream flow velocity.

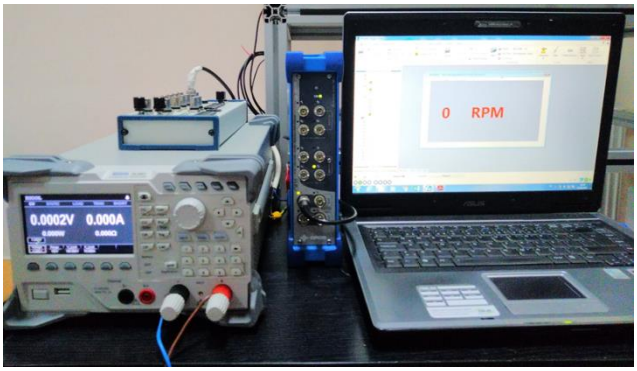

Fig. 2. Electronical load and data logger used during the experiment.

2.1 Turbine

The VAWT which is investigated consist of three bladed rotors as demonstrated in figure 3. Side view of the turbine demonstrated at a and top view of it is at b. Turbine shaft is fixed by bearing from the lower and upper parts of the test area. The height of the blades, H and diameter of turbine, D varies between 270-360 mm and 180-270 mm respectively. As a result, aspect ratio, H/D=1, 1.5 and 2 values are obtained. The blade chord has been adjusted to 60 mm and has not been changed in all turbine structures. Aluminum struts of 3 mm thickness and 15 mm width were used to connect the blades to the shaft. All metal parts were constructed with laser cutting when blades produced in 3D printer with PLA filaments.

Although different miles were used for turbine, most of them caused uncertainty during rotation. However, carbon shaft that is best choice minimizes vibration, especially at high rotation speeds, resulting in more reliable results. The air entering the test zone rotates the turbine counterclockwise. As is known, this is about the positioning of the blades.

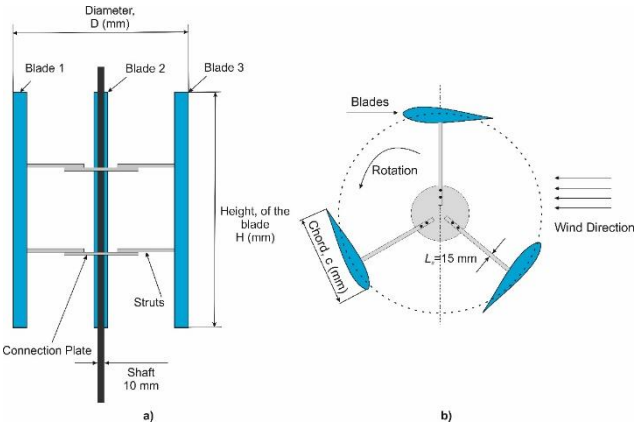

Fig. 3. Side view of the turbine a) and top view of the turbine b).

Figure 4 shows the details of connection struts and turbine blades. It has 120 mm diameters and 10 mm inner hole. There are four holes with a diameter of 3 mm each to screw the struts and plate together. Holes are specified from a to z with an angle of 5 degrees between them provided that only a-b is aligned. At each hole change, the blades have an angle of attack of 5 degrees. This produced part makes it very easy to give the turbine blades the angle of attack. At the same time, it minimizes the margin of error that may

Copyright © and. Published by Erciyes Energy Association

occur when angling the blades. Moreover, the figure 4 presents the profiles of the blades used in the experiment.

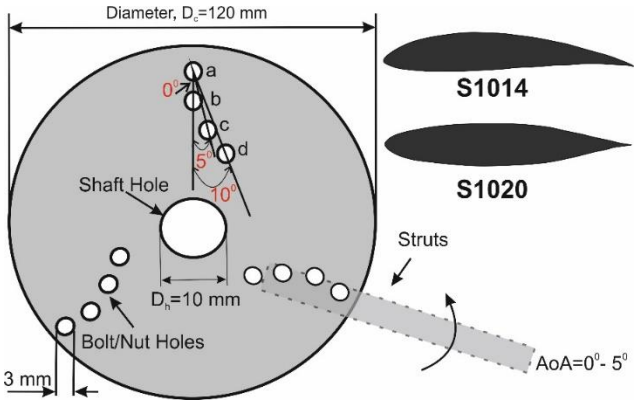

Fig. 4. Details of the connection plate and profile of blades.

A typical VAWT operates at low Tip Speed Ratios, TSR. For this reason, the wind speed has been tried to be kept in the closest possible range. In current experiment, the incoming flow speed was adjusted in the range of 4-9 m/s, and the inlet turbulence intensity is less than 1% normally when there is no vortex generator. The turbulence grid made from the metal material is located 350 mm from the front of the turbine. The main criterion for the grating's effect on flow is the porosity, β. This value can be calculated in equation 1 as given below. The porosity ratio was calculated according to equation 1 and it has 52%. Figure 5 represents the schematic view of the test set-up. The wind flow passes through the grid and reaches the turbine at a certain distance. d, expressing the turbulator diameter, was determined as 25 mm.

$$\boldsymbol{\beta = \frac{3a}{3a+b}} \qquad (1)$$

2.2 Test Facilities

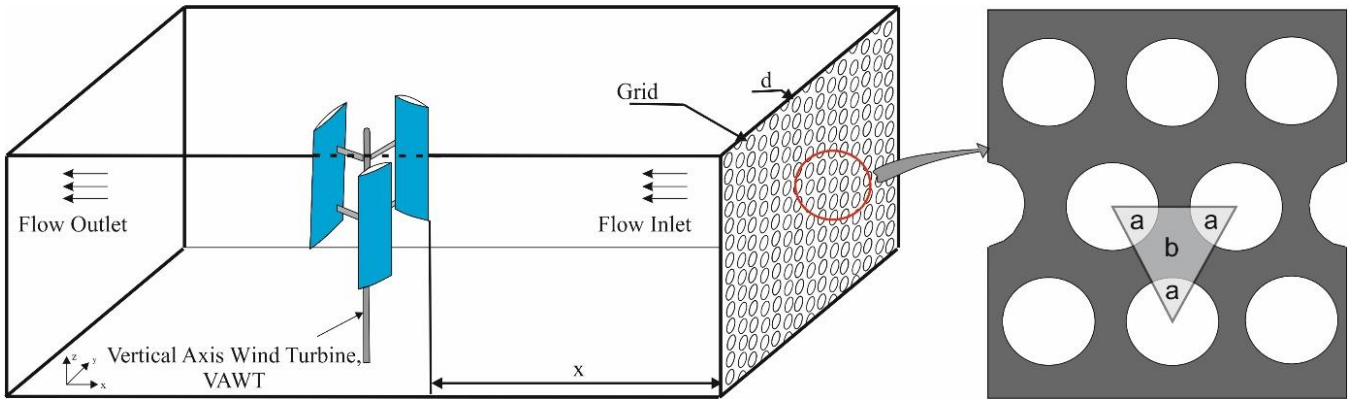

Fig. 5. Schematic representation of the test set-up and grid.

In order to calculate turbulence at first fluctuation flow velocity must obtained. Using this velocity value equation 2, Root Mean Square of these, u_{rms} is obtained and turbulence intensity can be calculated by equation (3).

$$\boldsymbol{u_{rms} = \sqrt{\sum_{i=1}^{n} \frac{(U_i - \overline{U})^2}{n-1}}} \qquad (2)$$

$$\boldsymbol{Tu(\%) = \frac{u_{rms}}{\bar{U}} \times 100} \qquad (3)$$

Where U is free stream flow velocity.

During the experiment effect of the solidity ratio, S was investigated and compared in figure 12 and figure 13 for S1014 and S1020 respectively.

2.3. Determination of DC motor efficiency

In order to determine the efficiency of the DC motor in the experiment, combine system was used as shown below in figure 6 at Nigde Omer Halisdemir University Lab. To explain the parts specified, number 1) Control panel, 2) Driver of the control panel, 3) Electronic load, 4) Data logger, 5) DC motor, 6) Torqumeter, 7) Laser Tachometer and 8) Electric motor. Figure 6b shows a detail illustration of the apparatus's overall perspective and is circled in red.

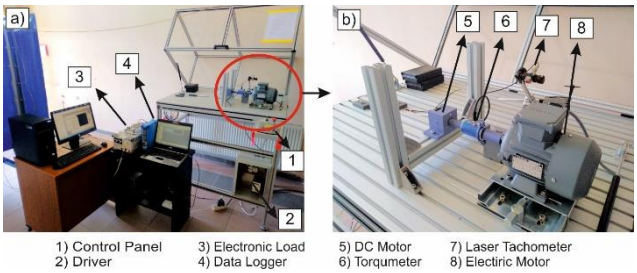

Fig. 6. Determination of DC motor efficiency set-up.

By changing the frequency through the control panel, the electric motor can be adjusted at the desired speed. In this step, motor rotation speed is set between 300 and 1800 rpm. The appropriate load is given according to the voltage value produced by the dc motor corresponding to each revolution. 10.000 number of samples were taken during the 10 seconds interval with 1000 sampling frequency per channel at the Oros data logger. These collected values were

averaged and an attempt was made to produce more precise and more accurate results. 5V input range was set to improve the accuracy of our results and 55P11, 1D probe was used to get only voltage as output.

3. RESULTS AND DISCUSSION

In this paper, the investigation of chord lengths, Angle of Attack, Aspect Ratio and presence of grid for the airfoils (S1014 and S1046) is done to get maximum output power from the wind turbine. When using two different airfoils, three different H/D ratios were formed with these blades, the blades connected to the system were tested at three different angles of attack with 0, 5 and 10 degrees and six different wind speeds varying between 4-9 m/s. Comparisons are made by repeating the same values of all these obtained values under turbulent flow.

The H/D for both blades in figure 7 can be regarded. At various flow velocities, this graph developed versus the coefficient of performance, Cp. As in this graph, complexity has been avoided by using the common value on the y axis in almost all other graphs. It is stated in figure 7 that as the H/D ratio increases, the performance coefficient increases, it is maximum at 1.5 and then decreases. The Cp value does not have a similar or specific relationship with the increase or decrease of wind speeds within the two wings. The only common situation is that it reaches its highest value at 1.5 H/D as mentioned earlier. Therefore, some graphs were created for 1.5 H/D ratio while other comparisons were made.

TSR versus Cp values were demonstrated in figure 8 at six different wind velocity. This comparison was made under the turbulence less than 1%. Although TSR (from 0.35 to 1.5) increases slightly as wind speed increases, the maximum Cp value has approximately the same values at 4, 5 and 6 m/s wind speeds. The highest Cp value was obtained at a speed of 8 m / s. In addition, wind speeds of 7, 8 and 9 m/s vary between 1 and 1.55 TSR for S1014. Similar trend applies to S1020. but has a lower performance curve than S1014. It has been observed that the Cp values change relatively less with the change of wind speed.

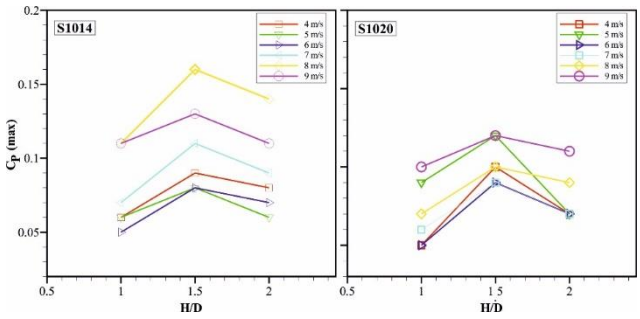

Fig. 7. Graphics of *H/D* ratios both *S1014* and *S1020* blade profile.

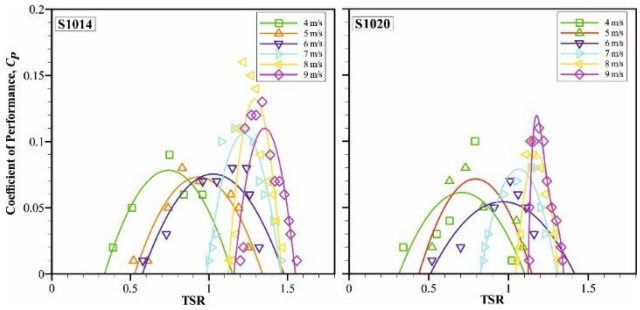

Fig. 8. Graphic of TSR versus Cp at different flow velocities.

Produced voltage, V (on the left), rotational speed, ω (in middle) and power, P (on the right) against to wind velocity for S1014 and S1020 were compared in figure 9 and figure 10 respectively. The red lines denoted by the square symbol in all figures indicate that turbulence is zero, and the green marked with a triangle means that turbulence corresponds to 5 percent. The purpose of expressing that turbulence is zero at this point and as shown in all graphs beyond is to express that it is below 1 percent. In other words, it is not working under zero turbulence, but a minimized state of turbulence in the wind tunnel. It is obvious that with increasing wind speed, all other outputs increase. Although the effect of turbulence seems to be small, change amounts are given for three separate points in the U∞-P graph.

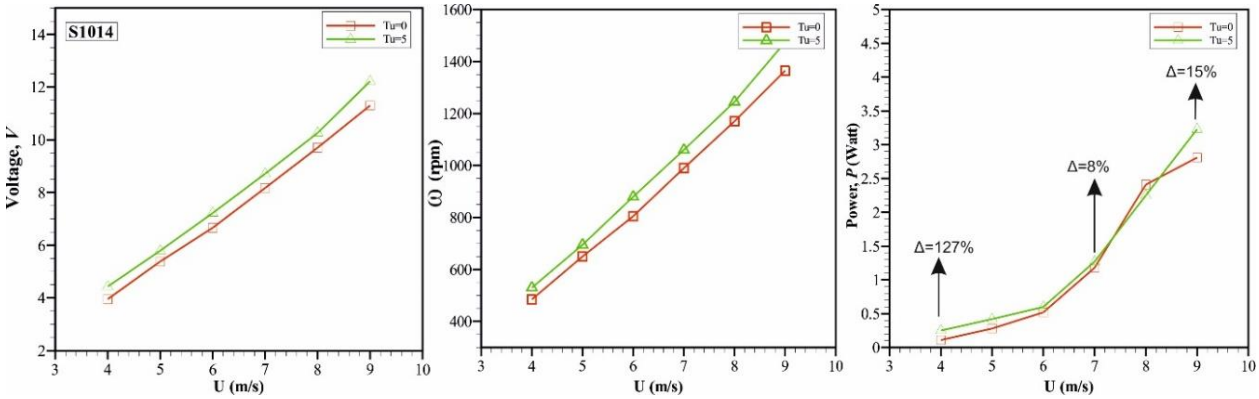

Fig. 9. Produced voltage, V, rotational speed, ω and power, P against to wind velocity for S1014.

Copyright © and. Published by Erciyes Energy Association

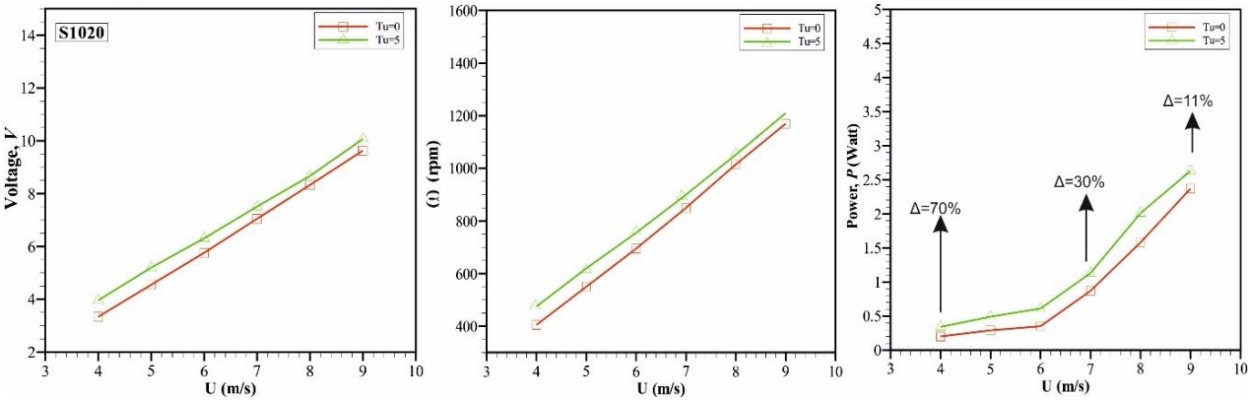

Fig. 10. Produced voltage, V, rotational speed, ω and power, P against to wind velocity for S1020.

In order to compare the power curves obtained under various angle of attack conditions, both turbulent and low turbulence conditions are plotted in Figure 11. S1014 blade profile is located on the left side of the graphic, while S1020 on the right. While the S1014 operates in the wider TSR range, the S1020 changes in the narrower. Increasing the turbulence for each velocity value has a positive effect on the performance coefficient. While the 5 and 10 degree of attack. Similar behavior was seen by S1014, although S1020 showed various differences, leading experts to conclude that 10 degrees was preferable. This is particularly evident at a free stream flow velocity of 8 m/s. Although the net Cp values at 8 m/s wind velocity are higher in S1014, the rate of increase is almost 23% and they are very close to each other.

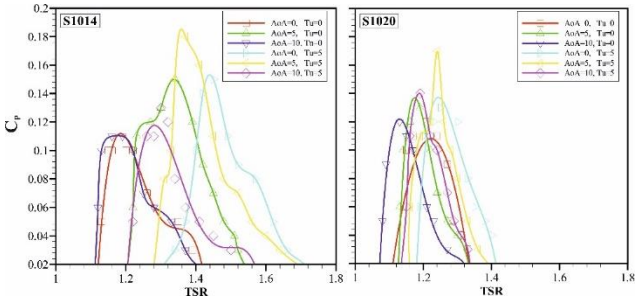

Fig. 11. Representation of TSR versus Cp according to Angle of Attack, AoA.

Figure 12 and figure 13 are related to the solidity ratio and is determined according to the aspect ratio. The effect of Solidity, S was evaluated by plotting the power curves for S1014 and S1020 in figure 12 and figure 13, respectively. Solidity of the wind turbine can be calculated from the equation 4 as shown below.

$$S = \frac{Nc}{\pi D} \qquad (4)$$

Where;

N is number of the blade, c is chord length and D is diameter of the turbine rotor.

It behaved differently at lower TSRs as a result of the increase in solidity. As can be understood from the turbulent situation with green lines and supporting figure 7, the maximum Cp was observed at S = 0.29, in other words at H/D=1.5. As the solidity rate increases in the S1020 profile, it shifts the operating range towards the lower region, although it does not narrow the working zone. Also proportionally, again at H/D = 1.5, there is the highest Cp change especially for S1020.

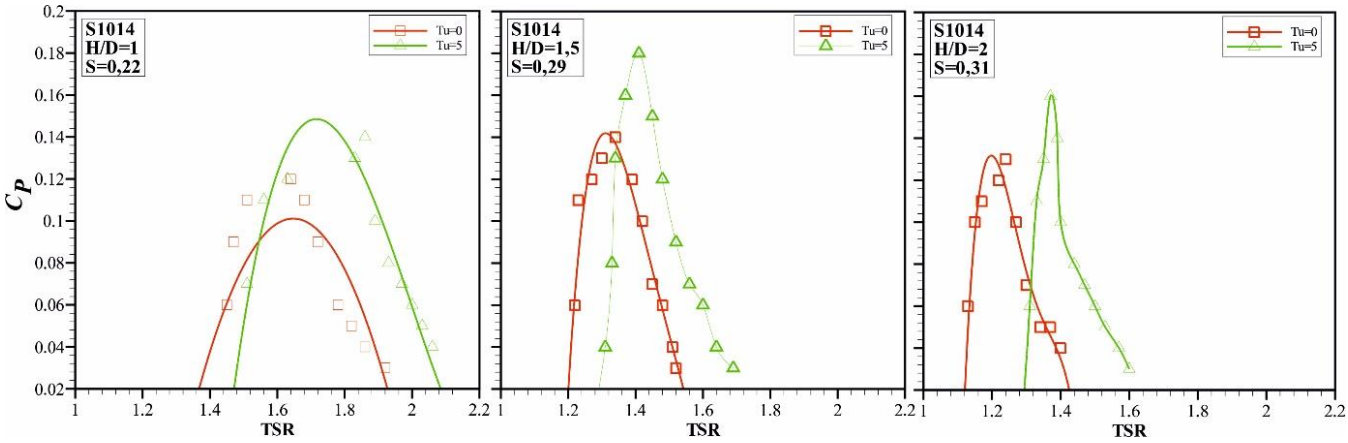

Fig. 12. Presentation of TSR versus Cp at different solidity for S1014.

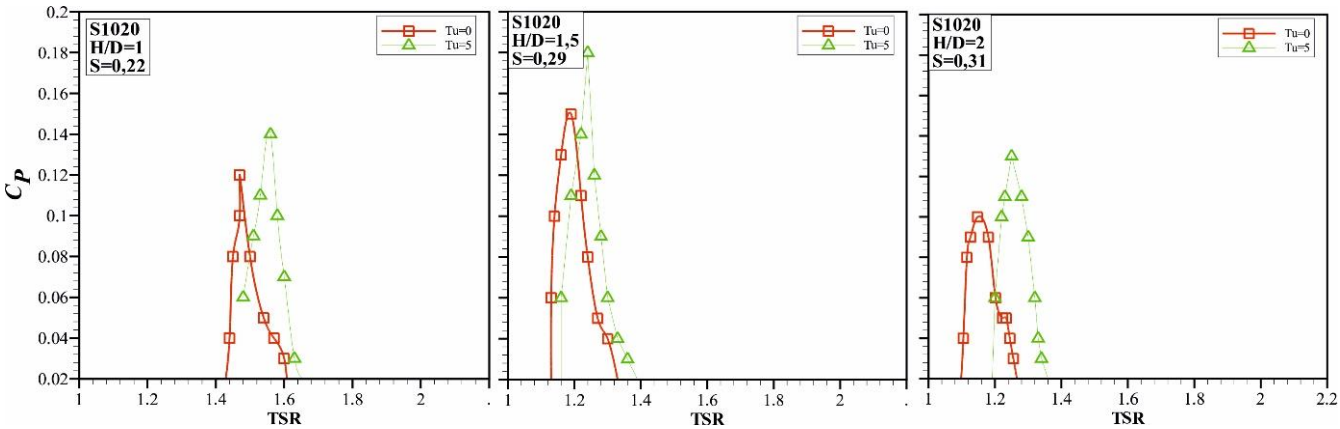

Fig. 13. Presentation of TSR versus Cp at different solidity for S1020.

Figure 14 contains all wind speed values (from 4 to 9 m/s) and allows comparisons with each other for both profile with presence of turbulence or not. To investigate the influence among the three parameters (turbulence, blade profile and wind velocity) only changes CP of each curve versus TSR is presented. green and red lines show S1014 while blue and turquoise colored lines represent S1020. It can be clearly seen that the increase in wind speed increases the Cp value, but it is observed that it does not change linearly when viewed as a ratio. Also, it is possible to obtain Cp close to 0.20 with increasing wind speed. At the same time, the increase in wind speed has narrowed the TSR range in which the turbine operates. As with all other graphs, this graph proves that the effect of turbulence is definitely positive for the performance coefficient. There is a dependence between Cp and TSR and it is an undeniable fact that turbulence has a positive effect on different blade models even though it has a different effect on this dependence.

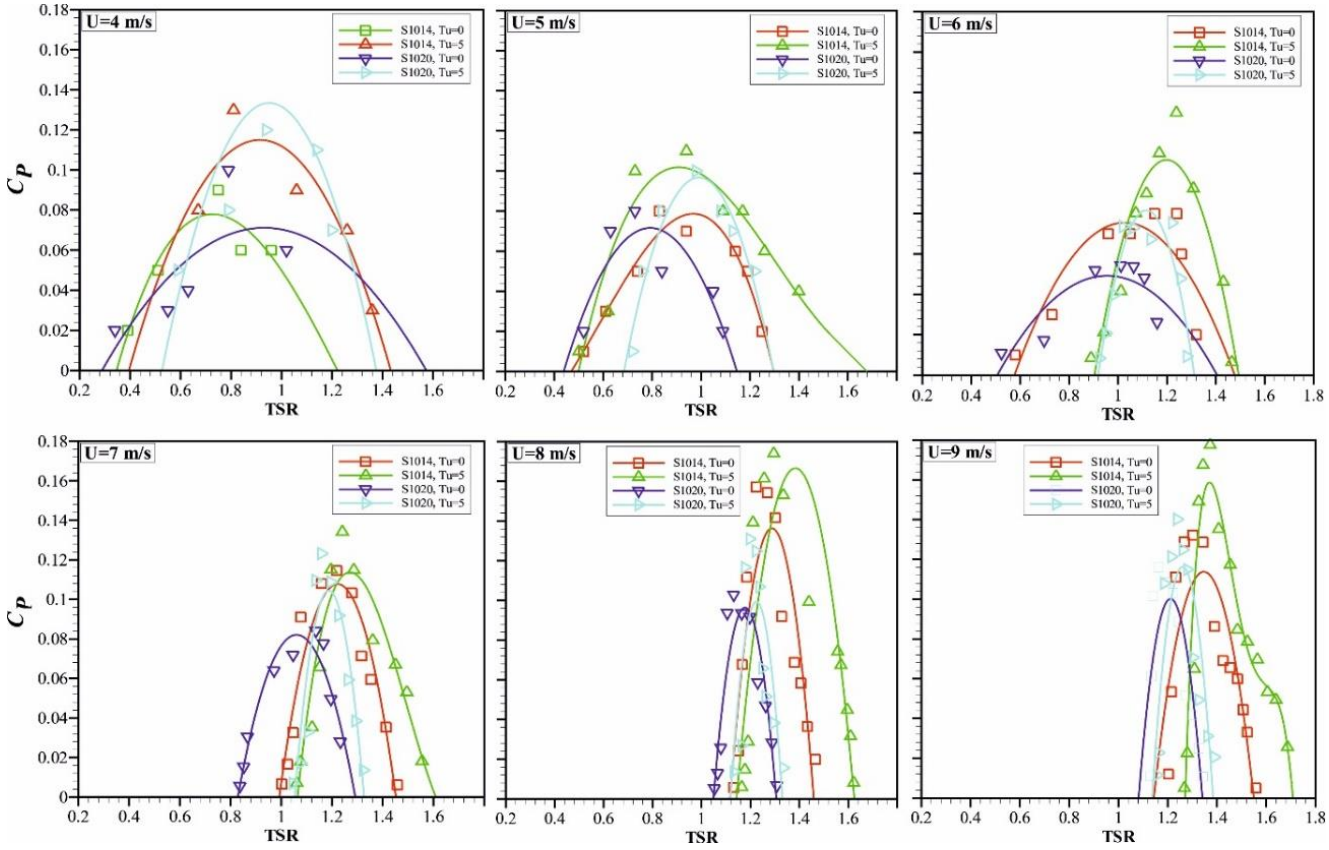

Fig. 14. Presentation of TSR versus Cp at different free stream flow velocity

4. CONCLUSION

Understanding the physics of air flow remains complex. Therefore, harvesting from wind energy could not reach the desired level. Researchers, engineers and scientists have many studies on this subject. If production and accessibility costs can be reduced rather than high performance, it will be seen among alternative and renewable energy sources in many parts of the world.

In this study, the performance of wind turbines designed according to two different blade profiles has been investigated by changing the different parameters in turbulent and low turbulence conditions. The findings obtained have been listed below.

Copyright © and. Published by Erciyes Energy Association

i. Two different blade profiles called S1014 and S1020 were produced in the 3D printer and used in the turbine.
ii. The rotor diameter, D was changed by keeping the turbine height, H constant and three different H/D ratios were determined as 1, 1.5 and 2.
iii. Chord length was kept constant as 60 mm. Therefore, only aspect ratio influenced on solidity, S.
iv. Three different angles of attack, AoA=0, 5, 10 have been examined.
v. Six different free stream flow velocities ranging from 4 to 9 m/s have been set.
vi. The vortex generator with 52% porosity value, β was placed in the test area and all experiments were carried out both with low and high turbulence levels.
vii. For both blade types, the highest Cp value was observed at the level of H/D=1 and therefore at S=0.29.
viii. Overall, the S1014 performed better in almost most experiments.
ix. Since the grid used makes the flow on the turbine distorted, fluctuated and turbulent, it has increased the performance coefficient.

In the future, it is planned to examine the aerodynamic performances of the modified blade, and it is also planned to conduct studies in a wider sense using optimization algorithms.

Conflicts of Interest

There is no conflict of interest.

Acknowledgments

The present work is supported by The Scientific and Technological Research Council of Turkey, TUBITAK project no:315M478 and Erciyes University, FDK-2019-9685. The authors would like to thank their support.

Nomencleature

H	**:**	Height of Blade (mm)
D	**:**	Diameter of Turbine (mm)
D	**:**	Diameter of Grid Hole (mm)
H/D	**:**	Aspect Ratio (-)
x	**:**	Grid Distance (mm)
Cp	**:**	Power Coefficient (-)
λ	**:**	Tip Speed Ratio (-)
T	**:**	Torque (Ncm)
n	**:**	Number of Revolution (rpm)
S	**:**	Solidity (-)
Ls	**:**	Strut Length (mm)
U_{∞}	**:**	Free Stream Velocity (m/s)
ω	**:**	Angular Velocity (rad/s)
R	**:**	Radius of Turbine (mm)
D_C	**:**	Diameter of Connection Plate (mm)
D_h	**:**	Hole Diameter on Connection Plate (mm)
AoA	**:**	Angle of Attack (Degree)
C	**:**	Chord length of blade (mm)
β	**:**	Porosity (-)
u'	**:**	Fluctuation Velocity
Tu	**:**	Turbulence Intensity
u_{rms}	**:**	Root Mean Square of Velocity Fluctuation

REFERENCES

[1] Wekesa D. W., Wang C., Wei Y. and Danao L.A.M. 2014. "Influence of operating conditions on unsteady wind performance of vertical axis wind turbines operating within a fluctuating free-stream: a numerical study." *Journal of Wind Engineering Industrial Aerodynamics* 135 76–89.

[2] Li Y. and Willman L. 2014. "Feasibility analysis of offshore renewables penetrating local energy systems in remote oceanic areas- A case study of emissions from an electricity system with tidal power in Southern Alaska." *Applied Energy* 117(15):42–53. http://dx.doi.org/10.1016/j.apenergy.2013.09.032.

[3] Kumar R., Raahemifar K. and Fung A.S. 2018. "A critical review of vertical axis wind turbines for urban applications." *Renewable Sustainable Energy Review* 89:281–91. http://dx.doi.org/10.1016/j.rser.2018.03.033.

[4] Stathopoulos HA T., Al-Quraan A., Bert Blocken A.D., Paraschivoiu M., Pragasen P. 2018. "Urban wind energy: Some views on potential and challenges." *Journal of Wind Engineering Industrial Aerodynamics* 179:146–57.

[5] Wekesa D.W., Wang C., Wei Y., Kamau J. N., and Danao L.A.M. 2015. "A numerical analysis of unsteady inflow wind for site specific vertical axis wind turbine: a case study for marsabit and garissa in kenya." *Renewable Energy* 76 32–45.

[6] Scheurich F., Brown R.E. 2013. "Modelling the aerodynamics of vertical-axis wind turbines in unsteady wind conditions." *Wind Energy* 16 91–107.

[7] Sallah M.B., Kamaruddin N. M., Kassim Z. M. and Abu Bakar E. 2021. "Experimental investigation on the characterization of self-starting capability of a 3-bladed Savonius hydrokinetic turbine using deflector plates." *Ocean Engineering* 228 108950, https://doi.org/10.1016/j.oceaneng.2021.108950

[8] Kacprzak K., Liskiewicz G. and Sobczak K. 2013. "Numerical investigation of conventional and modified Savonius wind turbines." *Renewable Energy* 60 578–585.

[9] Ajedegba J. O. 2008. "Effects of blade configuration on flow distribution on flow and power output of a Zephyr vertical axis wind turbine." Ph.D. thesis. University of Ontario Institute of Technology.

[10] Pallotta A., Pietrogiacomi D. and Romano G. P. 2020. "HYBRI e A combined Savonius-Darrieus wind turbine: Performances and flow fields." *Energy* 191 116433, https://doi.org/10.1016/j.energy.2019.116433.

[11] Krishnan A. and Paraschivoiu M. 2016. "3D analysis of building mounted VAWT with diffuser shaped shroud." *Sustainable Cities and Society* 27:160–6. http://dx.doi.org/ 10.1016/j.scs.2015.06.006.

[12] Bhuyan S. and Biswas A. 2014. "Investigations of self-starting and performances of simple h and hybrid h-Savonius vertical axis wind rotors." *Journal of Energy Conversion and Management* 87 859–867.

[13] Biswas A., Gupta R. and Sharma K. K. 2007. "Experimental investigation of overlap and blockage effects on three-bucket Savonius rotors" *Journal of Wind Engineering Industrial Aerodynamics*. 31 363–368.

[14] Gupta R., Biswas A. and Sharma K. K., 2008. "Comparative study of three-bucket Savonius rotor with combined three-bucket-Savonius-three-bladed-Darrieus rotor." *Journal of Renewable Energy Aerodynamics* 33 1974–1981.

[15] Sengupta A. R., Biswas A. and Gupta R. 2016. "Studies of some symmetrical and unsymmetrical blade h-darrieus rotors with respect to starting characteristics, dynamic performances and flow physics in low wind streams." *Renewable Energy* 93 536–547.

[16] Jeon K. S., Jeong J. I., Pan J.-K. and Ryu K.W. 2015. "Effects of end plates with various shapes and sizes on helical savonius wind turbines." *Renewable Energy* 79 167–176.

[17] Laín S., Taborda M., and López O. 2018. "Numerical study of the effect of winglets on the performance of a straight blade Darrieus water turbine." *Energies* 11:297. https:// doi.org/10.3390/en11020297.

[18] Elkhoury M., Kiwata T. and Aoun E. 2015. "Experimental and numerical investigation of a three dimensional vertical-axis wind turbine with variable-pitch." *Journal of Wind Engineering Industrial Aerodynamics* 139:111–23. https://doi.org/10.1016/j.jweia.2015.01.004.

[19] Lin S., Lin Y., Bai C. and Wang W. 2016. "Performance analysis of vertical-axis-wind-turbine blade with modified trailing edge through computational fluid dynamics." *Renewable Energy* 99:654–62. https://doi.org/10.1016/j.renene.2016.07.050.

[20] Chen J., Chen L., Xu H., Yang H., Ye C. and Liu D. 2016. "Performance improvement of a vertical axis wind turbine by comprehensive assessment of an airfoil family." *Energy* 114:318–31. https://doi.org/10.1016/j.energy.2016.08.005.

[21] Mohamed M.H. 2012. "Performance investigation of H-rotor Darrieus turbine with new airfoil shapes." *Energy* 47:522–30. https://doi.org/10.1016/j.energy.2012.08.044.

[22] Zamani M, Nazari S., Moshizi S.A. and Maghrebi M.J. 2016. "Three dimensional simulation of Jshape-d Darrieus vertical axis wind turbine." *Energy* 116:1243–55. https://doi. org/10.1016/j.energy.2016.10.031.

[23] Takao M, Kuma H, Maeda T, Kamada Y, Oki M, and Minoda A. 2009. "A straight-bladed vertical axis wind turbine with a directed guide vane row – effect of guide vane geometry on the performance." *Journal of Thermal Science* 18:54–7. https://doi.org/10.1007/s11630-009-0054-0.

[24] Kim D and Gharib M. 2014. "Unsteady loading of a vertical-axis turbine in the interaction with an upstream deflector." *Experimental Fluids* 55:1658. https://doi.org/10.1007/s00348-013-1658-4.

[25] Jeon J. H. and Kim S. H. 2018. "Optimization of thick wind turbine airfoils using a genetic algorithm" *Journal of Mechanical Science and Technology* 32 (7) 3191~3199.

[26] Kim D. and Gharib M. 2013. "Efficiency improvement of straight-bladed vertical-axis wind turbines with an upstream deflector." *Journal of Wind Engineering Industrial Aerodynamics* 115:48–52. https://doi.org/10.1016/j.jweia.2013.01.009.

[27] Hashem I and Mohamed M.H. 2018. "Aerodynamic performance enhancements of H-rotor Darrieus wind turbine." *Energy* 142:531–45. https://doi.org/10.1016/j. energy.2017.10.036.

[28] Malipeddi AR, Chatterjee D. 2012. "Influence of duct geometry on the performance of Darrieus hydroturbine." *Renewable Energy* 43:292–300. https://doi.org/10.1016/ j.renene.2011.12.008.

[29] Dabiri J.O. 2011. "Potential order-of-magnitude enhancement of wind farm power density via counter rotating vertical-axis wind turbine arrays." *Review Science Instrumentation* 77:3A–303A. https://doi.org/10.1063/1.3608170.

[30] Zanforlin S, Nishino T. 2016. "Fluid dynamic mechanisms of enhanced power generation by closely spaced vertical axis wind turbines." *Renewable Energy* 99:1213–26. https://doi.org/10.1016/j.renene.2016.08.015.

[31] Parneix N, Fuchs R, Immas A, Silvert F. 2016. "Efficiency improvement of vertical-axis wind turbines with counter-rotating lay-out." Wind Europe Summit 2016.

[32] Yang Yang1 Chun Li, Wanfu Zhang, Xueyan Guo and Quanyong Yuan, 2017. "Investigation on aerodynamics and active flow control of a vertical axis wind turbine with flapped airfoil." *Journal of Mechanical Science and Technology* 31 (4) 1645~1655.

[33] Sagharichi A, Zamani M, Ghasemi A. 2018. "Effect of solidity on the performance of variable-pitch vertical axis wind turbine." *Energy* 161:753–75. https://doi. org/10.1016/j.energy.2018.07.160.

Copyright © and. Published by Erciyes Energy Association